Progress In Electromagnetics Research B, Vol. 1, 219–235, 2008

MEANDERED SLOT AND SLIT LOADED COMPACT MICROSTRIP ANTENNA WITH INTEGRATED IMPEDANCE TUNING NETWORK

A. Kaya

Department of Electronics and Communication
Engineering Süleyman Demirel University
Isparta, Turkey, 32260

Abstract—In this paper, novel compact broadband dual frequency microstrip antennas are presented and broad-band impedance matching is proposed as a method for improve the matching level of antennas. The first proposed design consists of a rectangular microstrip antenna with a pair of parallel slots loaded close to the radiating edge of the patch and three meandering narrow slots embedded in the antenna surface. The second proposed design consists of a rectangular microstrip antenna with a meandering slits. With the first proposed design a size reduction of 34% and 45% for the two resonant frequencies is obtained respectively. The two frequencies have an operation frequency ratio of 1.30 and 1.25. The theoretical design implementation of compensated compact rectangular microstrip antennas with new configuration Pi-matching networks was presented. A new compensation network consisting of RC Mutator circuit and discrete capacitors are employed at the input of the microstrip antenna operating at 1.5 GHz and 2.5 GHz. The performance parameters of the designed microstrip antenna with and without compensation network were compared. The results show that compensation network can improve the return loss level and the resonant frequency can be controlled in a wide RF band.

1. INTRODUCTION

In recently, there have been many studies on compact microstrip antennas due to the increasing demand small antennas for personal communication equipment [1–6]. Compact operation of microstrip antennas can be obtained by meandering the radiating patch [1, 5, 6]. A slot and slit loaded rectangular microstrip antenna with dual-frequency

operation has recently been reported [3, 6, 16, 18]. The TM01 and TM30 modes are similar and have parallel polarization planes in these antennas. In addition, these two modes can be excited with good impedance matching using single probe feed. This indicates that a large antenna size reduction can be obtained by using the proposed design. In this paper, details of the proposed compact dual-frequency design have been described, and experimental results have been presented and discussed.

Conventional microstrip antennas in general have a conducting patch printed on a grounded microwave substrate, and have the attractive features of low profile, light weight and conformability to mounting hosts. In addition, applications in present-day mobile communication systems usually require smaller antenna size in order to meet the miniaturization requirements of mobile units. Thus, size reduction and bandwidth enhancement are becoming major design considerations for practical applications of microstrip antennas. For this reason, studies to achieve compact and broadband operations of antennas have greatly increased [6, 7]. Much significant progress in the design of compact microstrip antennas with broadband, dual frequency, dual-polarized and gain-enhanced operations have been reported over the several years [8, 15, 18]. In this paper, novel compact broadband dual frequency microstrip antennas are presented and broad-band impedance matching is proposed as a method for improve the matching level of microstrip antennas.

Different techniques are proposed to improve the return loss and control the resonant frequency in microstrip antennas. Short circuit loading or capacitive loading techniques have been proposed in literature [12] and obtained good results with these techniques but at the same time radiation pattern is changed. Attachment of lossless matching network for impedance matching is also commonly utilized technique to improve the bandwidth. In [9, 13] it is shown that utilizing transistors in the matching network, amplification and the matching function can be combined. In the following, the compact design combining the techniques of meandering and compensated network with pi matching for a microstrip antenna is demonstrated.

2. COMPENSATION NETWORK

It is evident that the calculated matching level is increased by using a reactive impedance matching network [9, 10, 11]. Ideally, this compensation network could transform the frequency dependent complex antenna impedance Z_{in} to a pure real resistance Z_0 over a large bandwidth as required as shown in Fig. 1. However, it is

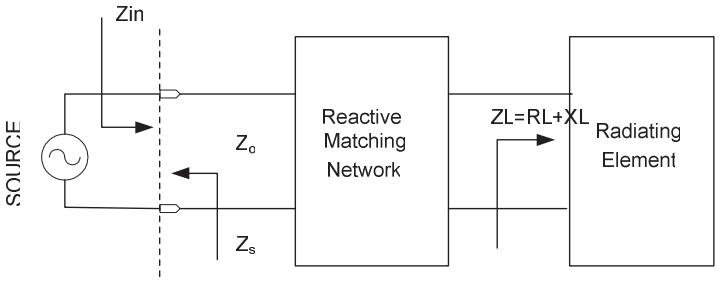

Figure 1. Broadband-matching system diagram.

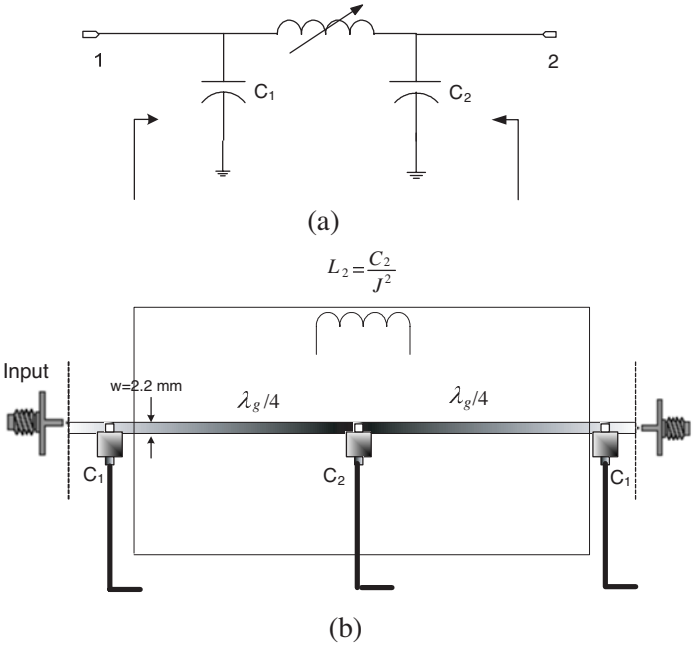

Figure 2. a) Starting matching network (b) Equivalent Pi-circuit topology.

not possible to realize a perfect match over a continuous band of frequencies by means of purely reactive (linear, passive losses) network. It is important that variable components are selected to optimize the matching level and maximize the bandwidth. The values of C_1, C_2, θ can be obtained by using the equations derived by the Y matrix for ideal transmission line is equated to the Y matrix for the circuit in Fig. 2(a), where θ is the electrical length. The steady state Y

parameters for an ideal transmission line are as follows:

$$Y = \begin{pmatrix} -\dfrac{j\cot(\theta)}{Z_0} & \dfrac{j\csc(\theta)}{Z_0} \\ \dfrac{j\csc(\theta)}{Z_0} & -\dfrac{j\cot(\theta)}{Z_0} \end{pmatrix} \tag{1}$$

The steady state Y parameters for the circuit in Fig. 1 are

$$Y = \begin{pmatrix} j\left(-\dfrac{1}{\omega L_2} + \omega C_1\right) & \dfrac{j}{\omega L_2} \\ \dfrac{j}{\omega L_2} & j\left(-\dfrac{1}{\omega L_2} + \omega C_1\right) \end{pmatrix}. \tag{2}$$

Equating terms in the Y matrices of (1) and (2) the two following unique equations are obtained:

$$j\left(-\frac{1}{\omega L_2} + \omega C_1\right) = j\left(\frac{-\cot(\theta)}{Z_0}\right) \tag{3}$$

$$j\left(\frac{1}{\omega L_2}\right) = j\left(\frac{\csc(\theta)}{Z_0}\right) \tag{4}$$

From (3) and (4) C_1, C_2 can be obtained as follows:

$$C_1 = \frac{-\cot(\theta) + \csc(\theta)}{\omega Z_0} \tag{5}$$

$$C_2 = \frac{J^2 \sin(\theta) Z_0}{\omega} \tag{6}$$

Conversely, one can solve for Z_0 and θ in terms of C_1 and C_2 as follows:

$$\theta = 2\arctan\left(\begin{array}{l} \dfrac{-J^2\sqrt{\dfrac{C_2}{-2J^2C_1 + \omega^2 C_1^2 C_2}}}{\omega C_2} + \omega C_1\sqrt{\dfrac{C_2}{-2J^2C_1 + \omega^2 C_1^2 C_2}} \\ +\sqrt{\dfrac{J^4}{-2J^2\omega^2 C_1 C_2 + \omega^4 C_1^2 C_2^2}} \end{array}\right) \tag{7}$$

$$Z_0 = \sqrt{\frac{C_2}{-\omega^2 C_1^2 C_2 + 2J^2 C_1}} \tag{8}$$

(7) and (8) are valid under the following circumferences:

$$0 < C_2 < \frac{J^2}{\omega^2 C_1} \qquad J\omega C_2 \neq 0 \qquad C_1\left(-2J^2 + \omega^2 C_1 C_2\right) \neq 0. \tag{9}$$

These network applications are very interesting because antennas cannot be considered as isolated elements and the impedance characteristics are changed with changing electromagnetic properties. When the input impedance varies, there is a mismatch between the front module and the antenna module. There are two major effects of this mismatch. First, the front module will not perform at the optimal efficiency under the load variations, and, second, the radiated power decreases due to the reflected power [9–11]. The result is an increase in the energy consumption or transmission quality deterioration. The L network, Pi network, and T network are used frequently in matching networks. Where the greater impedance matching flexibility or where the additional criteria are of significance, the Pi or T networks must be used [11]. The research reported here has concentrated on Pi network; however circuit analysis is just as applicable to the T network. The overall efficiency and the bandwidth performance of the matched antenna are generally best when the network is mounted as close as possible to the radiating element.

Electronically tunable capacitors are easily obtained but electronically tunable inductors are not easily achieved except MMIC process [12]. Unfortunately, tunable inductors have power and band limitations which may be prohibitive some certain applications. In MMIC design, spiral inductor is often used to reduce chip size. However, the area of a spiral inductor is still rather large compared to that of other lumped elements and the inductance values are related to physical structure.

In last a few years, microwave integrated circuit (MICs) and Monolithic circuits (MMICs) get the great advantages in a large RF system advantages. These circuits are used a lot in RF communication systems because of development of the system performances, become more reliable and having low cost. In this paper, theoretical and simulation studies have done on circuits shown in Fig. 2. To increase the gain and control the resonant frequency using the RC Mutator circuit is proposed as a MMIC circuit [13, 14]. The mutator is defined for the purpose of transforming one type of network element into another. An R-C mutator will transform a nonlinear resistor into a nonlinear capacitor, and vice versa. In matching network, system behaviors are examined by using R-C Mutator instead of the L_2 inductance. The equivalent circuit model of the matched antenna is shown in Fig. 3. To increase the gain and control the resonant frequency, an *R-C* Mutator circuit is proposed as a MMIC circuit [14] to realized electronically tunable C_2 capacitor. Hereafter capacitor can be controlled linearly. The *R-C* mutator can be built using only op amps operating high frequencies and linear passive resistors and capacitors. In the frequency domain, The Fig. 3's equation is

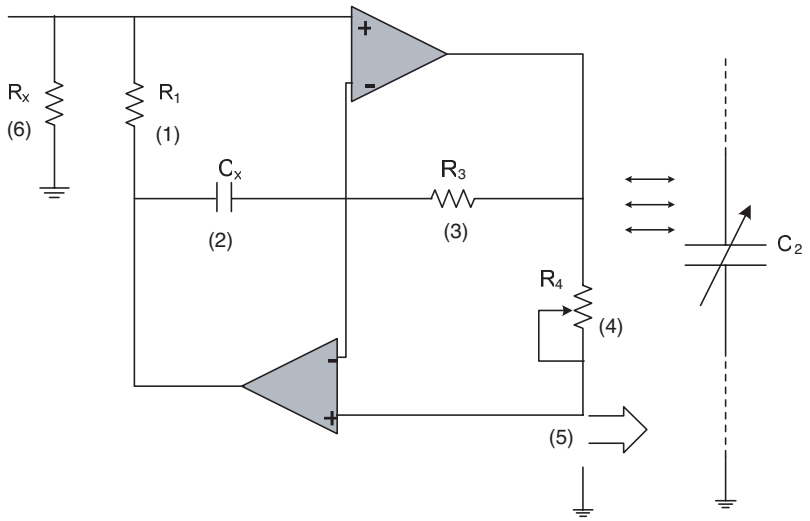

Figure 3. Configuration of *RC* Mutator.

equivalent to the following transmission matrix:

$$ABCD_{mutator} = \begin{pmatrix} 1 & 0 \\ 0 & \dfrac{G_1 G_3 R_4}{C_x s} \end{pmatrix} \tag{10}$$

$$ABCD_{Rx} = \begin{pmatrix} 1 & 0 \\ \dfrac{1}{R_x} & 1 \end{pmatrix} \tag{11}$$

In here, the *RC* mutator configuration is selected as shown in Fig. 3.

If the R_x resistor is connected to the input of the circuit shown in Fig. 3, the equivalent impedance of the *R-C* Mutator circuit can be written as

$$Z_{port} = \frac{G_1 G_3 R_4 R_x}{s C_x} \tag{12}$$

where G_1 and G_2 are the conductance values for R_1 and R_3 resistor.

The some C_2 values couldn't be obtained practically but with this technique can be possible as shown in Fig. 4. The *RC* mutator is used due to some of its advantages. *RC* mutator circuit can work on the high power application and the equivalent capacitance value (C) can be controlled only by the R value. The mutator circuit can be realized using MMIC process which enables easy compatibility with the rest of the system. This tuning network is efficiently used in a wide microwave frequency band. In this study, the *R-C* mutator circuit

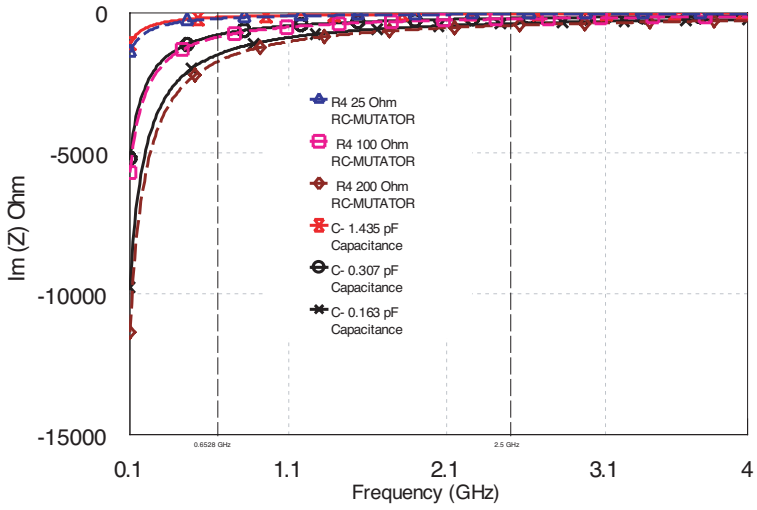

Figure 4. Comparison results of the R-C mutator and capacitor.

is simulated using the model in Fig. 2(b) which has $C_x = 3.3\,\text{pF}$, $R_1 = 10\,\Omega$, $R_3 = 100\,\Omega$, $R_x = 10\,\Omega$, resistor R_4 is the controlling parameter. The capacitor values obtained for the various R_4 values are depicted in Fig. 3.

The system return loss characteristics and input impedances are determined theoretically. Input impedance of this system represents Z_{in} and this impedance is given by (13)

$$Z_{in} = \frac{R_L}{\xi} + j \left(\begin{array}{l} \dfrac{X_L}{\xi} + \dfrac{\omega L_2}{\xi} - \dfrac{2\omega C_1 R_L^2}{\xi} - \dfrac{2\omega C_1 X_L^2}{\xi} - \dfrac{4\omega^2 C_1 L_2 X_L}{\xi} \\ -\dfrac{\omega^3 C_1 L_2^2}{\xi} + \dfrac{3\omega^3 C_1^2 L_2 R_L^2}{\xi} + \dfrac{3\omega^3 C_1^2 L_2 X_L^2}{\xi} \\ +\dfrac{2\omega^4 C_1^2 L_2^2 X_L}{\xi} - \dfrac{\omega^5 C_1^3 L_2^2 R_L^2}{\xi} - \dfrac{\omega^5 C_1^3 L_2^2 X_L^2}{\xi} \end{array} \right) \tag{13}$$

where

$$\xi = \left(2C_1 R_L \omega - C_1^2 L_2 R_L \omega^3\right)^2 + \left(1 + C_1^2 L_2 X_L \omega^3 - C_1 \omega (2X_L + L_2 \omega)\right)^2$$

The measurement, theoretical and simulated results for the reference antenna were presented as shown in Fig. 5.

The reflection coefficient Γ_{in} seen from the antenna system input terminals, can be defined in terms of the antenna impedances, Pi

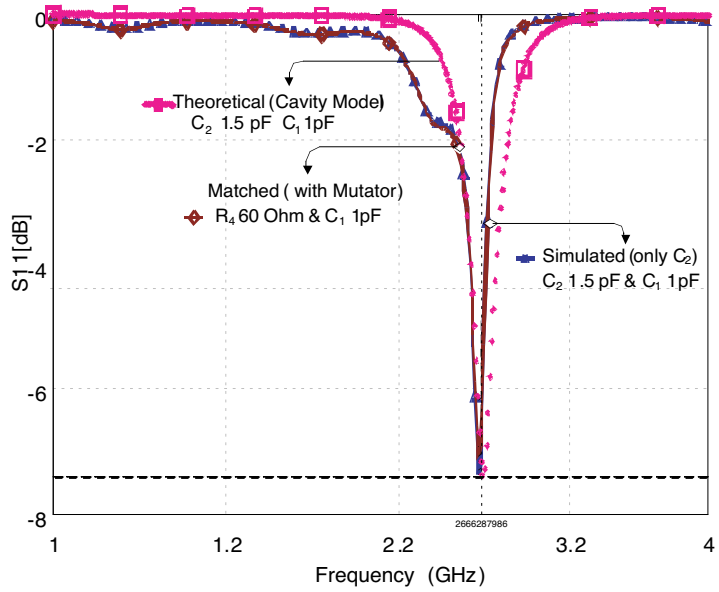

Figure 5. Simulation results for the compensated system (C_2 Mutator, and $C_1 = 1\,\text{pF}$) RMSA dimensions; $40 \times 40 \times 0.52\,\text{mm}$ & l (length) $20\,\text{mm}$ and $\varepsilon_r = 2.52$.

matching reactance's (C_1 and C_2) and the characteristic impedance Z_0 of the line as given below: (14)

$$\Gamma_{in} = \frac{\left(\begin{array}{r}\omega C_2(R_L + jX_L) + Z_0(J^2 Z_0(j - 2C_1\omega(R_L + jX_L))) \\ +C_2\omega(1 + C_1\omega Z_0(-j + C_1\omega(R_L + jX_L)))\end{array}\right)}{\left(\begin{array}{r}-\omega C_2(-j+C_1\omega Z_0)(-jR_L+X_L-jZ_0+C_1\omega Z_0(R_L+jX_L)) \\ +J^2 Z_0(2X_L - 2jR_L - jZ_0 + 2C_1\omega Z_0(R_L + jX_L))\end{array}\right)} \tag{14}$$

The $\Gamma_{opt}(f)$ is the reflection coefficient corresponding to maximum power transfer to the antenna. The resonant frequency and the bandwidth can be controlled by using Pi-matching network with tuning L_2 inductance and so does the reflection coefficient at the input antenna terminals such that $(\Gamma_{in}(f) = \Gamma_{opt}(f))$.

3. COMPACT MICROSTRIP ANTENNA DESIGN

The design consists of two parallel narrow rectangular slots etched in rectangular patch close to radiating edge and meandered with

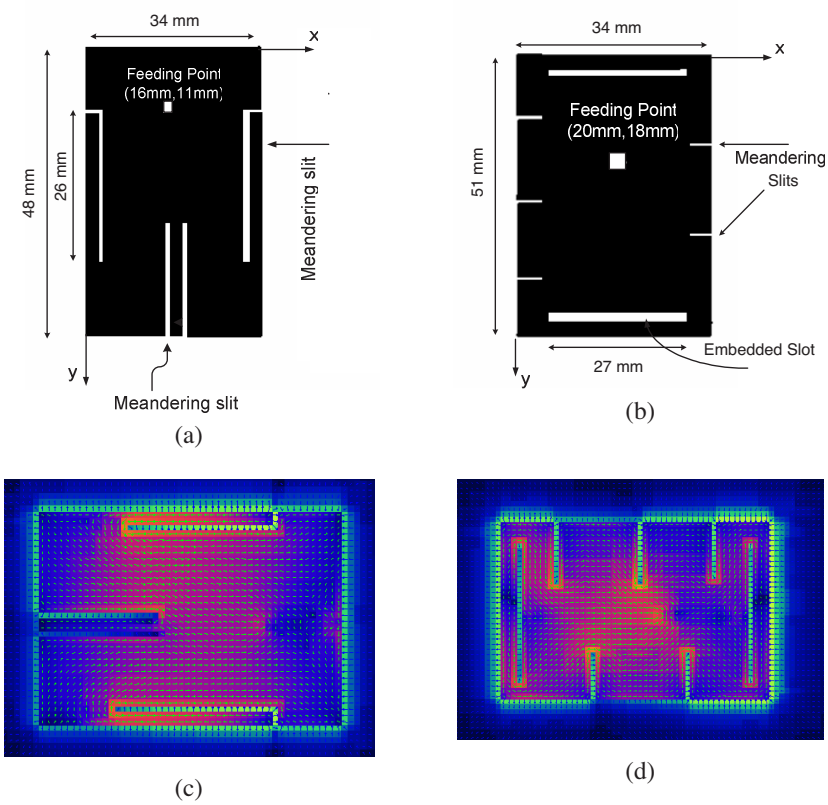

Figure 6. (a) Schematic layout of Compact I- Slotted geometry (b) Schematic layout of Compact II- RMSA with multiple slit and slotted geometry ($\varepsilon_r = 3.0$ & $h = 0.78$ mm; *TLC-32*) (c) and (d) Simulated surface current distributions in radiating patch 1.5 GHz and 2.5 GHz.

slits at the non-radiating edges. With the insetting slit, the two frequencies can be greatly lowered, which results in a large antenna size reduction for fixed dual frequency operation. By embedding suitable slots in a radiating patch, compact operation with an enhanced impedance bandwidth can be obtained. A typical design is shown in Fig. 6. However, the obtained impedance bandwidth for such a design is usually about equal to or less than 2.0 times that of the corresponding to conventional microstrip antenna. The first design, using three meandering slots on the surface a significant lowering of the both resonant frequencies is obtained with an enhanced operational bandwidth in comparison to standard rectangular microstrip antenna without slots.

3.1. Slot and Slit Loaded Antennas

In the study, TLYA-5CH200 substrate material manufactured by Taconic (a relative permittivity of 3.20 and a thickness of 0.80 mm) were used.

The Compact_I rectangular patch dimensions of $34 \times 48\,\text{mm}^2$ ($W \times L$), are selected along with the ground plane dimensions of $60 \times 60\,\text{mm}^2$. The Compact_II rectangular patch dimensions of $34 \times 51\,\text{mm}^2$ ($W \times L$), are selected along with the ground plane dimensions of $60 \times 60\,\text{mm}^2$. Based on the above designed concept, matched microstrip antenna with slots was constructed.

The slot length was fixed to be 26 mm for the Fig. 1(a) (Compact_I Antenna) and the slot length for the Fig. 1(b) (Compact_II Antenna) 27 mm. The probe-fed compact patch antennas are operated at 1.5 GHz and 2.5 GHz. The flowing surface currents on the geometries are important that is determined the radiation and the resonance characteristics as shown in Figs. 1(c), (d). The slot loaded patch is meandered by insetting five slits of length l and width w ($l \gg w$) at the non-radiating edges of the patch. With these slits excited surface currents paths of the TM_{10} and TM_{30} modes are lengthened, which effectively lowers the resonant frequencies of f_{10} and f_{30}. That is, a reduction in antenna size can be achieved for fixed dual-frequency operation. It should also be noted that the use of five slits for meandering the patch, instead of three slits as studied in [5, 6], is mainly to achieve good impedance matching. For the two slots, with dimensions $L_S \otimes W_S$, near the radiating edges of the patch, the design criteria given in [4, 12] are considered. The slot length is selected as $\sim$0.79 times the radiating length (W), and the distance between the slot and the radiating edge is chosen to be 2 mm (0.006 Lp) in this study in Type II.

3.2. Return Loss and Radiation Pattern

These antennas impedance variations of versus frequency are shown in Fig. 7(a). There are two or more frequencies. When the antenna is loaded with the pairs of $27 \times 1\,\text{mm}^2$ slots and pairs of slits $9 \times 1\,\text{mm}^2$, the frequency of operations are 2 and 2.5 GHz as shown in Fig. 7(b) but return loss level isn't enough for efficient operations. The return loss level can be increased by using proposed pi-matching circuit mentioned above.

When the antenna that it is called Compact_I antenna is loaded with pairs of $24 \times 1\,\text{mm}^2$ slots, the resonant frequency of operation decreases to 1.5 GHz, that is, about of 45% reduction in the frequency.

From the orientation of the fields in the radiating slot of the

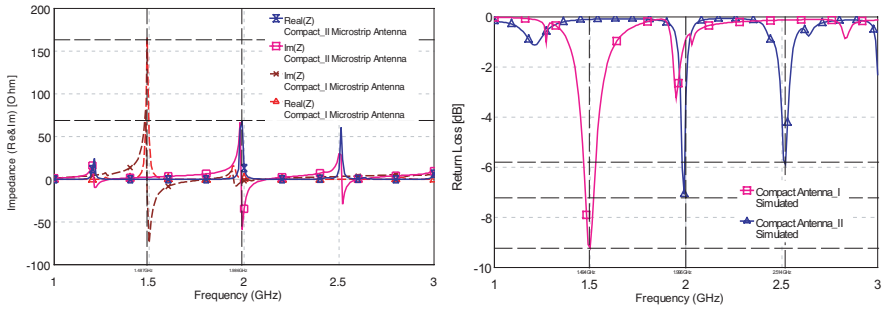

(a) (b)

Figure 7. (a) Simulated input impedance and (b) Return loss parameter ($\varepsilon_r = 3.0$ & $h = 0.78$ mm; *TLC-32*).

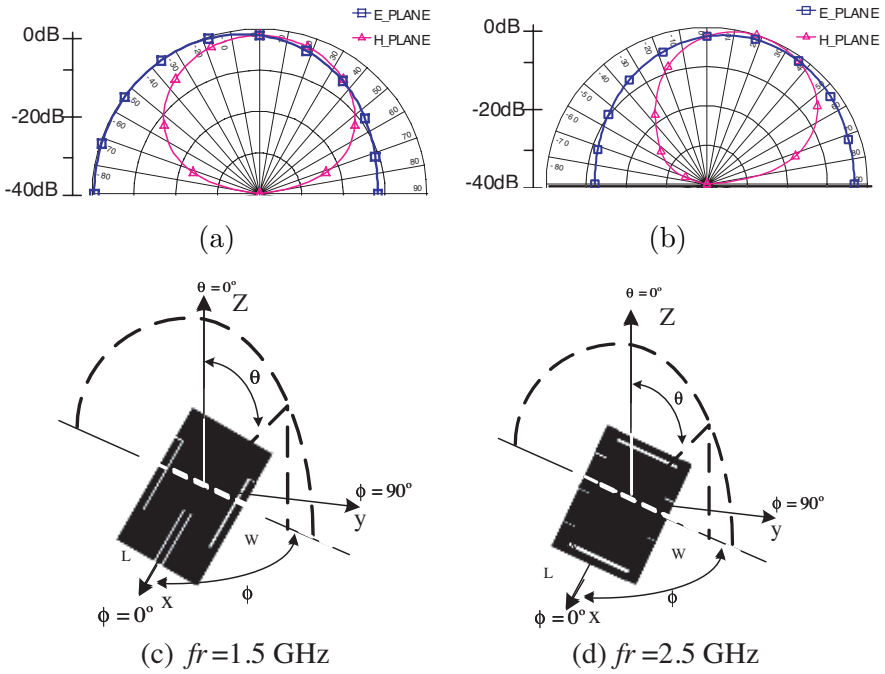

(a) (b)

(c) *fr* =1.5 GHz (d) *fr* =2.5 GHz

Figure 8. E and H plane radiation pattern at 1.5 GHz and 2.5 GHz.

antenna the E-plane refers to the xz-plane and the H-plane the yz-plane. The radiation patterns for these planes are plotted in Fig. 8. It is clearly seen that the radiation patterns aren't symmetric because of the surface wave currents.

3.3. Measurement Results

The antenna return loss parameter is measured using HP 8592B Spectrum Analyzer. Measurements are held using HP 8592B Spectrum Analyzer, HP8350B Sweep Generator via an IEEE 488 interface board attached to a PC and validated by Matlab script runs on this PC (all peripherals are GPIB devices).

The measurement return loss and transmission parameters are shown in Fig. 9 for the two type compact antennas. There are little differences between the simulated and the measurement data as shown in Fig. 9 and Fig. 7(b). This difference occurs due to some circumferences such as laboratory and manufacturing tolerances. For the measurement transmission parameter, the antenna geometry is mounted on a $60 \times 60\,\mathrm{mm}^2$ metallic plane.

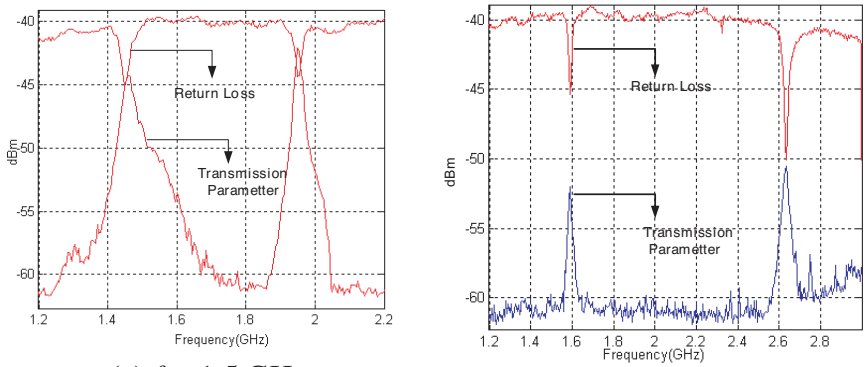

(a) fr =1.5 GHz (b) fr =2.5 GHz

Figure 9. (a) Measured return loss and transmission parameter of Compact_I antenna (b) Measured return loss and transmission parameter of Compact_II antenna.

4. COMPENSATED COMPACT MICROSTRIP ANTENNA

When the matching circuit connected to the antenna, the results are shown in Figs. 10 and 11, and the results are summarized in Table 1 and Table 2. These results will be changed when the feeding-point positions are changed. However, slits lengths, slots lengths and meandering slots dimensions are important. Return loss level is increased using compensated system realized by RC mutator.

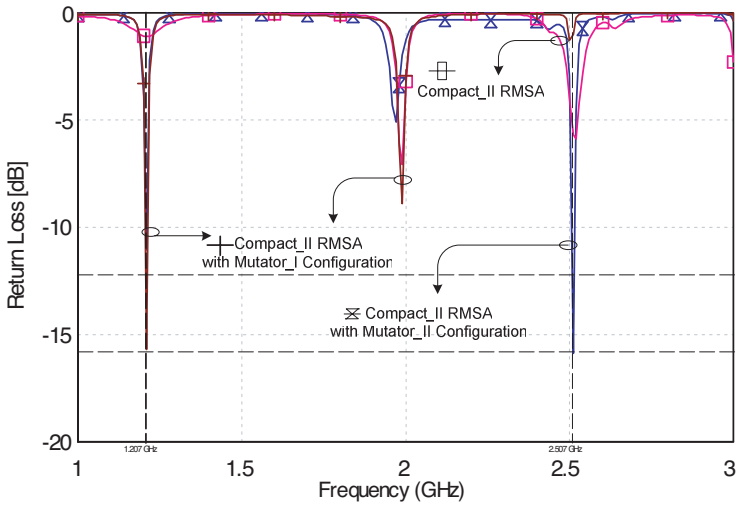

Figure 10. Simulation results for the compensated system (C_2 mutator, and $C_1 = 2\,\text{pF}$) RMSA dimensions; $51 \times 34 \times 0.78$ and $\varepsilon_r = 3$; *TLC-32.*

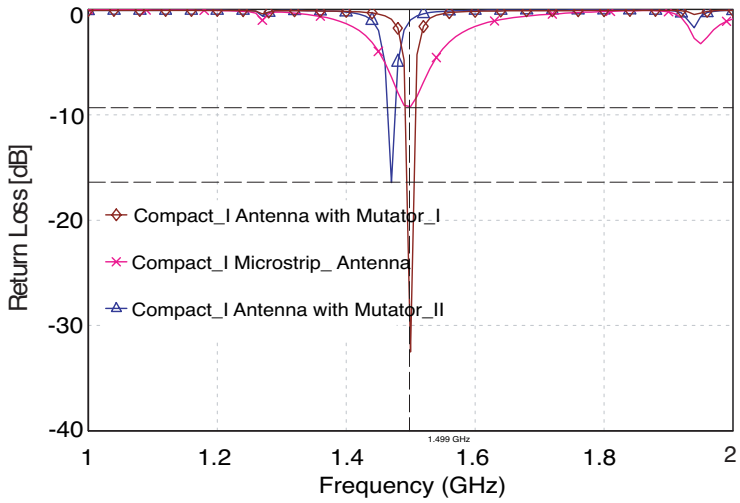

Figure 11. Simulation results for the compensated system (C_2 mutator, and $C_1 = 2\,\text{pF}$) RMSA dimensions; $48 \times 34 \times 0.78$ and $\varepsilon_r = 3$.

Table 1. *RC* mutator configuration.

Mutator_I Configuration for the Compact_II Antenna (f=1.21 GHz & S_{11}=-15.14 dB)					
$C_x pF$	$R_1\ \Omega$	$R_3\ \Omega$	$R_x\ \Omega$	$R_4\ \Omega$	$C_{eq}F$
1.65	10	25	10	10	$4.125\ 10^{-12}$
Mutator_II Configuration for the Compact_II Antenna (f=2.51 GHz & S_{11}= -15.76 dB)					
1	10	25	10	12	$2.08\ 10^{-12}$

Table 2. *RC* mutator configuration.

Mutator_I Configuration for the Compact_I Antenna (f=1.5 GHz & S_{11}=-32.53 dB)					
$C_x pF$	$R_1\ \Omega$	$R_3\ \Omega$	$R_x\ \Omega$	$R_4\ \Omega$	$C_{eq}\ F$
4	10	25	10	10	$10\ 10^{-12}$
Mutator_II Configuration for the Compact_I Antenna (f=1.47 GHz & S_{11}=-16.39 dB)					
5	10	10	50	110	$9.09\ 10^{-14}$

The return loss characteristics $|S_{11}|$ for both the reference and the compensated antennas are shown in Fig. 10(a). When the pi matching circuit is used as a compensated network, the resonant frequency can be controlled.

Results clearly indicate that, with increasing R_4, the resonant frequency of the meandered patch decreases as shown in Fig. 10 and Fig. 11. From the results for the case of Compact_I, microstrip antenna has a resonant frequency 1.5 GHz and for the case of Compact_II 2.5 GHz and can be changed by controlling the R_4 value. The slot width has a small effect on the resonant frequency.

For a conventional patch antenna (without a meandering slit and slots), the resonant frequency can be higher.

The return loss level is increased for compact II antenna configuration and the results are summarized in Table 1.

It is also seen that there are two resonant frequencies in Fig. 12 for the type II and there are large impedance changing in Compact_I RMSA configuration. The frequency-ratio range is about 1.25 in Compact_II RMSA. It can be noted that the matching network should

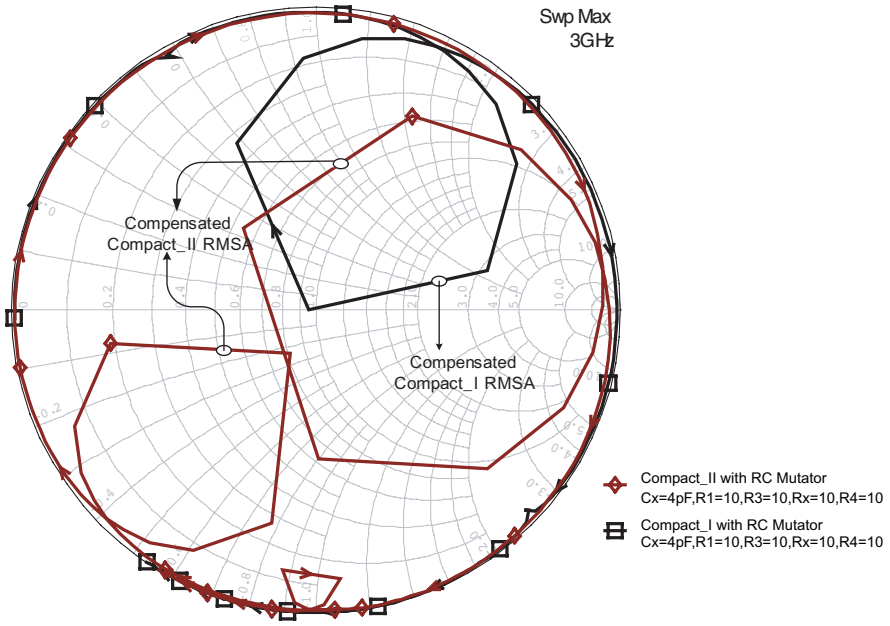

Figure 12. Smith chart of input impedance (C_2 mutator, and $C_1 = 2\,\text{pF}$).

be carefully chosen in according to the application.

The reference antenna has a return loss level is $-5.9\,\text{dB}$ at the resonant frequency. This value is not enough to define the impedance bandwidth (VSWR<2 or return loss level $<-10\,\text{dB}$), therefore it can be say that the antenna does not work well due to mismatch situation. However, this value can be increased to -15.14 and $32.53\,\text{dB}$ by utilizing the Pi matching network with *RC* mutator circuit. Tunable compensated microstrip antennas are of interest in many systems as they can be tuned over a large frequency range as shown in Figs. 10–11. Finally, the matching level is increased in compensated compact antenna with *RC* mutator and the resonant frequency can be controlled with only resistive components.

5. CONCLUSIONS

In this paper, a compact dual-frequency design using meandered rectangular patches has been successfully demonstrated. An experimental and theoretical investigation of the frequency dependence of the operational characteristics of compact microstrip antennas

shows that the impedance variations are the dominant mismatch factor, whereas the gain and radiation pattern variations are negligible in the wide impedance bandwidth. The performance parameters of the designed rectangular microstrip antenna with and without compensation networks have been compared using Microwave Office simulation program. A new circuit for designing a tunable impedance transformer has been demonstrated. The results show that the compensation network can improve the return loss level controlling the R_4 component with a minimum deep point of -32.53 dB. The system performance such as impedance bandwidth and matching level are improved using this new proposed network configuration with RC mutator.

REFERENCES

1. Wong, K. L. and S. C. Pan, "Compact triangular microstrip antenna VLF antenna modeling," *Electron. Lett.*, Vol. 33, 433–434, 1997.
2. Tang, C. L., H. T. Chen, and K. L. Wong, "Small circular microstrip antenna with dual frequency operation," *Electron. Lett.*, Vol. 33, 1112–1113, 1997.
3. Kuo, J. S. and K. L. Wong, "A compact microstrip antenna with meandering slots in the ground plane," *Microwave Opt. Techn. Lett.*, Vol. 29, 95–97, 2001.
4. Zhao, G., F.-S. Zhang, Y. Song, Z.-B. Weng, and Y.-C. Jiao, "Compact ring monopole antenna with double meander lines for 2.4/5 Ghz dual-band operation," *Progress In Electromagnetics Research*, PIER 72, 187–194, 2007.
5. Liu, W. C. and Y. T. Kao, "CPW-FED compact meandered strip antenna on a soft substrate for dualband WLAN communication," *Journal of Electromagnetic Waves and Applications*, Vol. 7, 987–995, 2007.
6. Shynu, S. V., G. Augustin, C. K. Aanandan, P. Mohanan, and K. Vasudevan, "Design of compact reconfigurable dual frequency microstrip antennas using varactor diodes," *Progress In Electromagnetics Research*, PIER 60, 197–205, 2006.
7. Wang, Y. J. and C. K. Lee, "Compact and broadband microstrip patch antenna for the 3g IMT-2000 handsets applying styrofoam and shorting-posts," *Progress In Electromagnetics Research*, PIER 47, 75–85, 2004.

8. Elsadek, H. and D. Nashaat, "Quad band compact size trapezoidal PIFA antenna," *Journal of Electromagnetic Waves and Applications*, Vol. 21, 865–876, 2007.
9. Mingo, J., A. Valdovinos, A. Crepo, and P. Garcia, "An RF electronically controlled impedance tuning network design and its application to an antenna input impedance automatic matching system," *IEEE Trans. on Microwave Theory and Tech.*, Vol. 52, 489–492, 2004.
10. Pues, H. F. and A. R. Van de Capelle, "An impedance matching technique for increasing the bandwidth of microstrip antennas," *IEEE Trans. on Antennas and Propagation*, Vol. 37, 1345–1354, 1989.
11. Kaya, A., S. Kln, E. Y. Yüksel, and U. Cam, "Bandwidth enhancement of a microstrip antenna using negative inductance as impedance matching device," *Microwave and Optical Technology Letters*, Vol. 42, 476–478, 2004.
12. Thompson, M. and J. K. Fidler, "Determination of the impedance matching domain of impedance matching networks," *IEEE Trans. on Circuits and Systems*, Vol. 51, 2098–2106, 2004.
13. Goras, L., "Linear and nonlinear mutators derived from GIC-type configurations," *IEEE Trans. on circuits and systems*, Vol. 28, 165–169, 1981.
14. Antoniou, A., "Novel RC-active network synthesis using generalized immitance converters," *IEEE Trans. on Circuit Theory*, Vol. CT-17, 1970.
15. Bilotti, F., F. Urbani, and L. Vegni, "Design of an active integrated antenna for a PCMCIA card," *Progress In Electromagnetics Research*, PIER 61, 253–270, 2006.
16. Alkanhal, M. and A. F. Sheta, "A novel dual-band reconfigurable square-ring microstrip antenna," *Progress In Electromagnetics Research*, PIER 70, 337–349, 2007.
17. Afrooz, K., A. Abdipour, A. Tavakoli, and M. Movahhedi, "Time domain analysis of active transmission line using FDTD technique (application to microwave/mm-wave transistors)," *Progress In Electromagnetics Research*, PIER 77, 309–328, 2007.
18. Sadat, S., M. Fardis, F. G. Kharakhili, and G. Dadashzadeh, "A compact microstrip square-ring slot antenna for UWB applications," *Progress In Electromagnetics Research*, PIER 67, 173–179, 2007.